Final Draft
of the original manuscript:

Anisotropic stiffness and tensional homeostasis induce a natural anisotropy of volumetric growth and remodeling in soft biological tissues

F.A. Braeu[1], R.C. Aydin[1], and C.J. Cyron[2,3]

[1]Institute for Computational Mechanics
Technical University of Munich, Munich, Germany

[2]Institute of Continuum Mechanics and Materials Mechanics
Hamburg University of Technology, Hamburg, Germany

[3]Institute of Materials Research, Materials Mechanics,
Helmholtz-Zentrum Geesthacht, Geesthacht, Germany

Address for Correspondence:

Christian J. Cyron
Institute of Continuum Mechanics and Materials Mechanics
Hamburg University of Technology
Eissendorfer Strasse 42, 21073 Hamburg
christian.cyron@tuhh.de

Abstract

Growth in soft biological tissues in general results in anisotropic changes of the tissue geometry. It remains a key challenge in biomechanics to understand, quantify, and predict this anisotropy. In this paper, we demonstrate that anisotropic tissue stiffness and the well-known mechanism of tensional homeostasis induce a natural anisotropy of the geometric changes resulting from volumetric growth in soft biological tissues. As a rule of thumb, this natural anisotropy makes differential tissue volume elements dilate mainly in the direction(s) of lowest stiffness. This simple principle is shown to explain the experimentally observed growth behavior in a host of different soft biological tissues without relying on any the additional heuristic assumptions or quantities (such as ad-hoc defined growth tensors).

1 Introduction

In biological tissues one frequently observes growth, that is, production or degradation of tissue mass along with directly associated changes of the tissue geometry. Growth can be divided into two categories. Surface growth results from deposition of mass on external or also internal surfaces of tissues or organs. Examples are the growth of biofilms, horns, nails, hair or seashells (Skalak, Farrow et al. 1997, Soleimani, Wriggers et al. 2016). By contrast, in volumetric growth material is deposited throughout the whole volume of tissues. For example, growth of collagenous soft tissues results from collagen production by smooth muscle cells or fibroblasts distributed all over the volume of, for example, blood vessels or tendons (Humphrey, Dufresne et al. 2014). If mass is produced in a differential tissue volume element, the volume element in general has to expand in order to accommodate the additional mass. Therefore, volumetric growth is usually modeled as a local inelastic dilatation (Rodriguez, Hoger et al. 1994) of differential tissue volume elements. This dilatation is in general anisotropic (i.e., unequal in different spatial directions) as illustrated also in Figure 1. Its anisotropy plays a key role in soft tissue biomechanics. For example, it enables arteries to increase wall thickness under increased blood pressure. Without such ability, arteries might be prone to rupture in particular in early life where the shape of and load on tissues and organs changes continuously and considerably. For developing theoretical and computational models of volumetric growth in soft biological tissues it is thus essential to understand and quantify the factors governing the anisotropy of the geometric changes induced by growth.
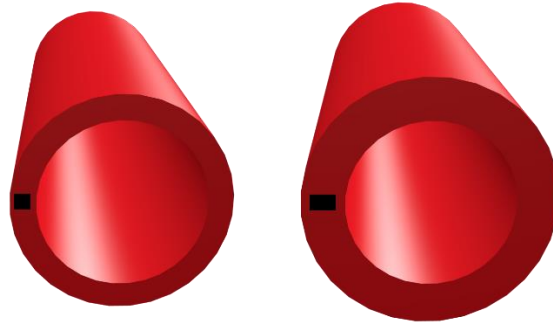
Figure 1. If blood pressure in an artery (left) is increased, the wall thickens (right). Thereby differential volume elements (black) dilate not isotropically (i.e., equally in circumferential direction and wall-thickness direction) but anisotropically (i.e., mainly in wall-thickness direction). This way, differential volume elements with initial square cross section become rectangular with an elongated side in wall-thickness direction. So far, the origin of this anisotropy and similar other observations related to volumetric growth in soft biological tissues remains poorly understood.

Theoretical and computational models of the growth and remodeling of living soft tissues have attracted rapidly increasing attention over the last decade (Goriely and Vandiver 2010, Karšaj, Sorić et al. 2010, Grytz, Meschke et al. 2011, Grytz, Sigal et al. 2012, Valentín, Humphrey et al. 2013, Grytsan, Watton et al. 2015, Lindquist Liljeqvist, Hultgren et al. 2016, Braeu, Seitz et al. 2017, Virag, Wilson et al. 2017). Recently, there have been attempts to inform such models by experiments measuring the in general anisotropic changes of tissue geometry during growth (Tsamis, Cheng et al. 2012). However, the natural difficulties to obtain such information in vivo limit the application of such approaches so far significantly. Therefore, theories have been developed how anisotropic shape changes of differential volume elements might be defined in the absence of specific experimental information. (DiCarlo and Quiligotti 2002, Ambrosi and Guana 2007) proposed the hypothesis that they might be governed by an Eshelby-like stress tensor. Despite its theoretical elegance this approach is currently not widely used, possibly because of its difficulties to explain without further assumptions the experimentally observed growth behavior in important situations, for example, in blood vessels in hypertension. As a consequence, currently most theoretical and computational models of volumetric growth of soft living tissues still rely on mainly heuristic assumptions about the anisotropy of the geometric changes resulting from the growth process. These assumptions are usually simply made such that reasonable results are obtained in the end. Obviously, this prevents truly predictive simulations. Moreover, simplistic assumptions such as the one of isotropic growth are widely used but render for many relevant applications results that are in strong disagreement with experimental observations as pointed out in (Braeu, Seitz et al. 2017).

It is thus widely acknowledged that there remains a pressing need for a theory that can predict the anisotropy of the changes of the tissue geometry resulting from volumetric growth in soft biological tissues in good agreement with experimental observations and on the basis of some fundamental mathematical or mechanical ideas (Ambrosi, Ateshian et al. 2011). Such a theory could significantly help to understand the geometric evolution of living organisms during morphogenesis early in life as well as the mechanobiological adaptation processes in adult tissues, for example, in aneurysmatic or hypertensive blood vessels (Eriksson, Watton et al. 2014, Sáez, Peña et al. 2014, Grytsan, Watton et al. 2015, Grytsan, Eriksson et al. 2017, Lin, Iafrati et al. 2017). Moreover, it could provide a powerful tool for

the development of new and efficient methods in tissue engineering, a field where volumetric growth processes are of particular importance. Finally, it could be key to understand the interplay between mechanical and chemical factors (e.g., genetic factors) governing soft tissue growth.

In this paper, we examine the problem of volumetric growth specifically in soft biological tissues subject to tensional homeostasis. Tensional homeostasis is a mechanism that relies on a coupling between mechanics and biology and seeks to establish or maintain in tissues some preferred mechanical state (Cyron and Humphrey 2017). It can be expected to govern growth and remodeling in load-bearing soft collagenous tissues such as blood vessels, tendons, the bladder or stomach as well as general connective tissue. Osseous tissues are not considered herein. Also nervous tissues is not considered here because the role of tensional homeostasis in such tissues is unclear to date.

In section 2 we first briefly delineate a general mathematical model of volumetric growth and remodeling in load-bearing soft biological tissues, largely in line with previous work. In section 3 we discuss the micromechanical and physiological foundations of growth and remodeling in soft biological tissues, in particular the production and degradation of tissue mass and the reorganization of the tissue microstructure following the principle of tensional homeostasis. In section 4 we demonstrate that anisotropic tissue stiffness and the mechanism of tensional homeostasis, which has been observed to be a fundamental property of various biological tissues, induce a natural anisotropy of volumetric growth in load-bearing soft biological tissues. As a rule of thumb, this natural growth anisotropy will make differential tissue volume elements dilate mainly in the direction(s) of lowest stiffness during volumetric growth. In section 5 we demonstrate how these ideas give rise to a new type of computational model that can capture volumetric growth and remodeling in a host of soft biological tissues without any ad-hoc definition of a growth tensor.

2   Continuum mechanics

Relying on the general theory of nonlinear continuum mechanics, we model soft biological tissues as mechanical bodies whose material points $X \in B_0$ are mapped at times $t \geq 0$ by a deformation to their current position $x(t, X) \in B(t)$, see also Figure 2. The Jacobi matrix of this deformation is the so-called deformation gradient

$$F = \frac{\partial x}{\partial X}. \tag{1}$$

The set of material points B_0 is called the reference configuration, and we note that this configuration need not be stress-free in general. Herein, we assume without loss of generality that the reference configuration is always identical to the initial configuration, that is, $B_0 = B(t = 0)$. Differential volume elements dV in the reference configuration B_0 are deformed into volume elements

$$dv = |F|dV. \tag{2}$$

in the current configuration $B(t)$ where $|F|$ is the determinant of F. Herein, we model biological tissues as so-called constrained mixtures. That is, we assume that the material in each volume element is a mixture of n constituents. For the i-th constituent, the deformation gradient can be split into an inelastic part F_{gr}^i and an elastic part F_e^i such that

4

$$\boldsymbol{F} = \boldsymbol{F}_e^i \, \boldsymbol{F}_{gr}^i. \tag{3}$$

Here, the inelastic part $\boldsymbol{F}_{gr}^i$ characterizes how the material of the i-th constituent in a volume element in the reference configuration would deform if it were cut out from its surrounding continuum and additionally separated from the other constituents in the mixture and thus not subject to any loading or confinement any longer (cf. Figure 2). $\boldsymbol{F}_{gr}^i$ captures inelastic changes of the stress-free configuration of the i-th tissue constituent due to growth and remodeling (Rodriguez, Hoger et al. 1994, Ambrosi and Guana 2007, Zöllner, Abilez et al. 2012, Braeu, Seitz et al. 2017, Grytsan, Eriksson et al. 2017, Kehl and Gee 2017, Truster and Masud 2017). The general idea to use an inelastic part of the deformation gradient to this end goes back to (Rodriguez, Hoger et al. 1994), which introduced Eq. (3) for the simple special case $n = 1$ so that only a single elastic and inelastic deformation tensor were required for the whole material. In general, the elastic state of the tissue material at each point is defined by $\boldsymbol{F}$ and $\boldsymbol{F}_{gr}^i$. In a given configuration the elastic part of the deformation gradient $\boldsymbol{F}_e^i$ may be different among the individual constituents. However, we yet assume that all constituents deform together, that is, all experience the same deformation increments over time and thus form a constrained mixture.
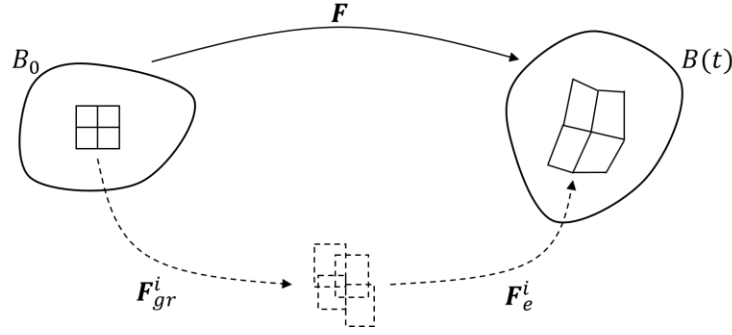
Figure 2. Illustration of the kinematics of volumetric growth and remodeling. The deformation gradient $\boldsymbol{F}$ can be split at each point into an inelastic part $\boldsymbol{F}_{gr}^i$ and an elastic part $\boldsymbol{F}_e^i$. The inelastic $\boldsymbol{F}_{gr}^i$ accounts for inelastic changes of the stress-free configuration of individual constituents in differential volume elements that may be associated with growth and remodeling. Volume elements in the reference configuration B_0 are deformed by $\boldsymbol{F}_{gr}^i$ into an intermediate configuration which is in general not geometrically compatible so that neighboring volume elements may overlap or form gaps. The elastic $\boldsymbol{F}_e^i$ applied to each differential volume element ensures that the total deformation gradient field is geometrically compatible (i.e., neighboring differential volume elements fit together without gaps or overlaps) and satisfies mechanical equilibrium in the current configuration $B(t)$.

Volumetric growth and remodeling in biological tissues happens slowly (typically on a time scale of hours, days, or months) and is thus modeled here as a quasi-static process so that the balance of linear momentum is

$$\mathrm{div}(\boldsymbol{P}) + \varrho_0 \boldsymbol{b}_0 = \boldsymbol{0} \tag{4}$$

with the total referential mass density of the mixture

$$\varrho_0 = \sum_{i=1}^{n} \varrho_0^i, \tag{5}$$

the mass density per unit reference volume of the i-th constituent ϱ_0^i, the body force vector $\boldsymbol{b}_0$ (per unit mass) and the first Piola-Kirchhoff stress tensor

$$\boldsymbol{P} = \frac{\partial \Psi}{\partial \boldsymbol{F}} \tag{6}$$

where

$$\Psi = \sum_{i=1}^{n} \varrho_0^i W^i \left(\boldsymbol{F}_e^i \right) + \Psi^\# \tag{7}$$

is the strain energy of the constrained mixture per unit volume. W^i is the strain energy of the i-th constituent per unit mass, which is assumed to depend only on its elastic deformation, that is, on $\boldsymbol{F}_e^i$. The special strain energy $\Psi^\#$ (per unit volume) is accounting for excluded volume interactions between the individual mass increments and microstructural elements forming the constrained mixture. Such interactions are often assumed to ensure in practice a (nearly) constant spatial density ϱ of all the constituents together at any time. With Eq. (4.6) from (Holzapfel 2000), this assumption is equivalent to

$$dv = \frac{\varrho_0(\boldsymbol{X},t)}{\varrho} dV \tag{8}$$

or, using (2) in (8),

$$\varrho = \varrho_0 / |\boldsymbol{F}| \,. \tag{9}$$

Therefore, $\Psi^\#$ can be modeled by a penalty-type energy

$$\Psi^\#(t) = \frac{\varepsilon}{2} \left(|\boldsymbol{F}(t)| - \frac{\varrho_0(t)}{\varrho} \right)^2 \tag{10}$$

with some very large ε. We note that $\Psi^\#$ in (7) is an important difference between the approach introduced herein and most previous work. Below we will demonstrate that one of its non-trivial consequences is that it implicitly defines the anisotropy of the geometry changes resulting from volumetric growth, which has to be defined so far mainly on the basis of heuristic assumptions.

If ϱ_0^i and $\boldsymbol{F}_{gr}^i$ are known, the unknown current deformation field $\boldsymbol{x}$ can be computed immediately at any point in time using (1), (3) and (5) − (7) in (4) so that the balance of linear momentum (4) can be written completely in terms of the unknown deformation field $\boldsymbol{x}$, yielding in d dimensions for the d unknown components of $\boldsymbol{x}$ a system of d coupled differential equations. The crucial difficulty is thus determining $\boldsymbol{F}_{gr}^i$ and ϱ_0^i at each point in time.

To determine ϱ_0^i, one typically assumes a known initial value and an evolution equation of the type

$$\dot{\varrho}_0^i = \varrho_0^i \, \boldsymbol{k}_\sigma^i : \Delta \boldsymbol{G}^i. \tag{11}$$

Here the over-dot denotes a time derivative, $\Delta \boldsymbol{G}^i$ is a mass production stimulus, for example the difference between the current stress or stretch and some homeostatic target value (cf. also Eq. (7) in (Cyron and Humphrey 2017)). The colon in (11) denotes a double contraction product and $\boldsymbol{k}_\sigma^i$ is a second

order gain tensor. In the literature different choices for $\Delta \boldsymbol{G}^i$ and $\boldsymbol{k}_\sigma^i$ can be found. While the exact parameter values used for these quantities differ significantly, there is yet a high overall similarity at least between the functional forms used.

The situation is much more involved for $\boldsymbol{F}_{gr}^i$, for which even the general functional form of the evolution equations and $\boldsymbol{F}_{gr}^i$ itself remain highly controversial to date. Helping to overcome this controversy can be considered a primary objective of this paper.

Remark 1: the number of constituents n depends on the mathematical model of growth and remodeling. In the recently developed homogenized constrained mixture models (Cyron, Aydin et al. 2016, Braeu, Seitz et al. 2017) or also in the recruitment stretch models following (Watton, Hill et al. 2004, Eriksson, Watton et al. 2014, Grytsan, Watton et al. 2015) n can be understood as the number of structurally different constituents such as elastin, smooth muscle and collagen (or also different collagen fiber families) that can be distinguished in a biological tissue. By contrast, when following the constrained mixture models based on multi-network theory, which were introduced by (Humphrey and Rajagopal 2002) and further used, for example, by (Wilson, Baek et al. 2012, Wilson, Baek et al. 2013), n in the above equation (7) should rather be understood as the number of mass increments with different stress-free natural configurations present in each differential volume element. Recalling that constrained mixture models based on multi-network theory keep track of differential mass increments deposited during each differential time interval, n is for these models in theory infinite. In computational implementations where time is discretized by a finite number of points in time, also n is finite but in practice often very large. We note that the ideas developed herein can be applied to any of the above mentioned models by simply incorporating in these models an interaction energy $\Psi^\#$ as in (7) and defining the evolution of $\boldsymbol{F}_{gr}^i$ according to the discussion below. Thereby the exact form of $\Psi^\#$ is largely irrelevant as long as it ensures a constant spatial density of the material (cf. (9)) sufficiently accurately.

3 Physiological foundations

To overcome the controversy how to compute $\boldsymbol{F}_{gr}^i$ we first briefly recall some physiological foundations of growth and remodeling. Noting the partially inconsistent nomenclature used in the literature, we start with a few definitions.

In the following, the term remodeling refers to an inelastic reorganization of the microstructure of the tissue. On the microscale, this reorganization is accomplished by biological cells rearranging the tissue fibers and altering also the inter-molecular connections within and between these fibers. The altered microstructure of the tissue will in general result in altered stress-free configurations of tissue material increments, that is, in an altered $\boldsymbol{F}_{gr}^i$ in Eq. (3). Tissue mass, however, is by definition not changed by remodeling.

In opposition to that, the term of growth refers in the following to the process of production or degradation of tissue mass as well as any elastic deformation of the tissue that is directly associated with this process. By definition, growth is understood in the following as a process during which the inter-molecular connections defining the stress-free configuration of tissue material remain unaltered. That is, growth is understood herein as a process not affecting $\boldsymbol{F}_{gr}^i$ in Eq. (3). It may rather be imagined as a kind

of elastic swelling.

In practice, growth and remodeling, in the sense of the above definitions, may occur simultaneously. For example, cells may produce additional collagen fibers. The additional fiber volume deposited thereby within the tissue will in the first place induce and elastic distension of the extant tissue (i.e., a kind of swelling). The fiber production and the associated elastic distension together are referred to as *growth* herein. However, while or directly after the cells are producing new fibers they may also alter the inter-molecular connections in the tissue, thereby changing the stress-free state of tissue material increments and thus *remodeling* the tissue. Obviously, growth and remodeling in the sense of the above definitions are physically per se independent processes and are thus to be treated separately also in mathematical modeling.

Relying on these definitions, this paper is based on two major hypotheses, which we first briefly introduce and then support by references to experimental observations reported in the literature.

Hypothesis 1: Remodeling is driven by tensional homeostasis only. We assume that cells remodel the surrounding tissue so as to maintain or achieve a preferred state of mechanical stress, which is called homeostatic state. Moreover, we assume that this mechanism, which is also called tensional homeostasis, is the only driver of remodeling.

Hypothesis 2: The spatial mass density remains constant during growth. We assume that the packing density of the fibers in the tissue does not change during growth, that is, it does not change when additional fibers are produced or extant fibers are degraded.

It is well-known that cells such as fibroblasts or smooth muscle cells have a natural tendency to reorganize surrounding collagen tissues towards a preferred mechanical state. To date it is not yet fully understood which mechanical quantity exactly (e.g., stress, stretch or stiffness) defines the target of this process. However, there is at least considerable evidence that it might be the stress in the tissue fibers or at least some closely related quantity (Brown, Prajapati et al. 1998, Ezra, Ellis et al. 2010). The reorganization of the tissue due to tensional homeostasis is well-known to imply also a reorganization of inter-molecular connections (Cyron and Humphrey 2017) and changes thereby the stress-free configuration of differential volume elements. While numerous papers have reported the phenomenon of tensional homeostasis, to the authors' best knowledge nobody has reported so far that deposition or degradation of tissue mass are directly associated with a specific kind of reorganization of inter-molecular connections in the tissue. Therefore, following Ockham's lex parsimoniae we assume Hypothesis 1.
(Cyron, Aydin et al. 2016, Braeu, Seitz et al. 2017, Cyron and Aydin 2017) demonstrated that remodeling due to tensional homeostasis can be captured by an evolution of the inelastic part F_{gr}^i of the deformation gradient following the equation

$$\left[\frac{\dot{\varrho}_0^i(t)}{\varrho_0^i(t)} + \frac{1}{T^i}\right]\left[S^i - S_{pre}^i\right] = \left[2\frac{\partial S^i}{\partial C_e^i}:\left(C_e^i L_{gr}^i\right)\right]_{F=const} \tag{12}$$

Therefore, Hypothesis 1 directly translates into the assumption that we can describe the evolution of F_{gr}^i in (3) by (12). In (12), $L_{gr}^i = \dot{F}_{gr}^i F_{gr}^{i-1}$ is the velocity gradient of the inelastic deformation. T^i is the average

survival time of tissue fibers and structural connections during the microstructural reorganization driven by tensional homeostasis. S^i is the second Piola-Kirchhoff stress of the i-th constituent, and $C_e^i = F_e^{iT} F_e^i$ its elastic Cauchy-Green deformation tensor with F_e^i from (3). S_{pre}^i is the 2nd Piola-Kirchhoff target stress of tensional homeostasis.

Hypothesis 2 was inspired by experimental observations reported, among others, by (Wolinsky and Glagov 1967, Matsumoto and Hayashi 1996). It was observed that the thickness of soft tissues such as arteries under increased load seems to adopt so as to maintain a certain preferred level of tissue stress. If, for example, blood pressure in an artery is increased, also its wall thickness increases until the original level of wall stress is restored. On the other hand, the observations reported by (Flynn, Bhole et al. 2010) suggest that fiber degradation in soft tissues strongly depends on the microscopic fiber stretch. This stretch can therefore also be expected to be restored by tensional homeostasis. However, tensional homeostasis can restore both fiber stress and fiber stretch at the same time only if fiber density in the tissue remains (approximately) constant during growth. This conclusion directly motivates Hypothesis 2 Mathematically, Hypothesis 2 means that (8) and (9) hold not only in the sense of an incompressibility condition during elastic deformation but also more generally during volumetric growth where they enforce a constant spatial mass density over time.

Remark 2: As discussed above, there is considerable experimental evidence supporting Hypothesis 1 and Hypothesis 2, which was the reason for choosing these two hypotheses as starting points for the theoretical discussion in this paper. Nevertheless, one should keep in mind that the amount of experimental observations shedding light on the physiological foundations of growth and remodeling in soft biological tissues is still very limited and so the hypotheses proposed and conclusions drawn in this paper certainly still require significant further examination in the future.

Remark 3: An essential feature of nearly all mathematical models of volumetric growth in soft biological tissues published so far (Rodriguez, Hoger et al. 1994, Ambrosi and Guana 2007, Zöllner, Abilez et al. 2012, Braeu, Seitz et al. 2017, Grytsan, Eriksson et al. 2017, Kehl and Gee 2017, Truster and Masud 2017) is the assumption that growth itself is directly associated with some inelastic reorganization of the tissue microstructure, represented by some growth tensor (i.e., a growth-induced inelastic part of the deformation gradient). This lead to an ongoing controversy how to define this growth tensor. The growth model proposed herein bypasses the definition of any inelastic growth tensor. The only inelastic part of the deformation gradient to be defined is the one related to remodeling for whose definition one can resort to rather general observations made in vitro on the remodeling of fibroblast-seeded tissue equivalents.

Remark 4: (Braeu, Seitz et al. 2017) suggested to capture the inelastic deformation by growth and remodeling via a multiplicative split $F_{gr}^i = F_r^i F_g^i$ with F_g^i capturing the inelastic deformation by growth and F_r^i capturing the inelastic deformation by remodeling. Mathematically, the approach introduced herein can be considered a special case of this concept with the particularly simple choice $F_g^i = I$, where I is the identity tensor.

Remark 5: the idea of treating growth and remodeling separately, which is essential in this paper, was, in some form, proposed already earlier by (DiCarlo, Naili et al. 2006) for osseous tissue and subsequently also by (Cyron, Aydin et al. 2016, Braeu, Seitz et al. 2017) for soft tissue.

(a)   (b)
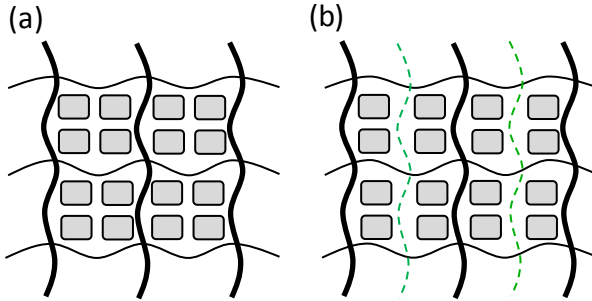
Figure 3: Deposition of new material during growth directly induces an elastic distension of differential tissue volume elements that can be understood as a form of elastic swelling. This swelling will create the space that is required to accommodate the additional mass by expanding the volume element predominantly in the direction(s) of lowest stiffness. Because in the direction(s) of lowest stiffness the extant fibers will oppose the deformation of the volume element by swelling only minimally. In (a) a differential volume element is illustrated whose stiffness in vertical direction is much higher than in horizontal direction (illustrated by much thicker load-bearing fibers in vertical direction). If in this volume element additional fibers are deposited, it will elastically dilate mainly in horizontal direction (b). This dilatation mainly in horizontal direction will trigger also remodeling (i.e., inelastic reorganization of the tissue) mainly in horizontal direction, leading finally to a long-term anisotropic inelastic deformation of the volume element mainly in horizontal direction.

4   Natural anisotropy of volumetric growth and remodeling

The constant spatial mass density assumed in Hypothesis 2 implies that growth is always associated with a change of tissue volume, a kind of elastic swelling of differential volume elements. At the same time, Hypothesis 1 implies that growth is not directly associated with any inelastic change of the tissue microstructure (i.e., any change of F_{gr}^i). Therefore, Hypothesis 1 and Hypothesis 2 together imply that growth becomes in the first place manifest as a kind of elastic distension of differential volume elements in the tissue. This elastic distension changes the stress field in the tissue and thereby triggers remodeling (i.e., inelastic reorganization of the tissue) due to tensional homeostasis. In this section, we will demonstrate that this setting gives rise to a natural anisotropy of the geometry changes induced by volumetric growth, which is mainly governed by the anisotropy of the elastic stiffness of the tissue. We will focus thereby on an (isolated) differential volume element to exclude confounding effects from the surrounding continuum and boundary conditions. We will perform our analysis in two steps. In the first step we will examine the elastic distension of the tissue directly associated with growth, in the second step the remodeling dynamics which it gives rise to.

Via (10), the amount of mass produced per differential volume element per unit time $\dot{\varrho}_0$ determines the ratio between the size of a differential volume element in current and reference configuration, that is, $|F(t)|$. The dilatation of differential volume elements during volumetric growth is illustrated in Figure 3. If new material is deposited in the tissue, the extant tissue will immediately dilate elastically in order to increase its volume and accommodate the additional material. The following discussion will demonstrate

that this dilatation is naturally anisotropic. To see this, we first note that via (10) and (12) volumetric growth itself (without the remodeling it may give rise to in the long term) alters $|\boldsymbol{F}(t)|$ but leaves $\boldsymbol{F}_{gr}^i$ in (3) constant, which means that the change of $|\boldsymbol{F}(t)|$ must be associated with some change of $\boldsymbol{F}_e^i$. Next we resort to the concept of traction-free configurations. In a constrained mixture of n constituents as assumed above in (7), different constituents may have different individual stress-free configurations. That is, in general there exists no configuration in which all constituents in a differential volume element are stress-free at the same time. However, there always exists a so-called traction-free configuration in which the average stress of the different constituents weighted with their respective volume fractions ϱ_0^i/ϱ_0 is zero. The traction-free configuration can be imagined as the configuration of a differential volume element into which it would naturally deform when cut out from its surrounding continuum and not subjected to any external load. Herein, we denote the tensor mapping infinitesimal line elements from (the tangent space of) the reference configuration to (the tangent space of) the current traction-free configuration by $\boldsymbol{F}_G$. If a differential volume element is traction-free in a certain configuration, this holds also after any rigid body rotation. To render the notion of the traction-free configuration unique, we thus define without loss of generality that $\boldsymbol{F}_G$ does not imply any rotation compared to the reference configuration. That is, $\boldsymbol{F}_G$ is symmetric and the rotation tensor resulting from its polar decomposition is simply the identity tensor. The evolution of the traction-free configuration in time can be described using the velocity gradient (Menzel and Kuhl 2012)

$$\boldsymbol{L}_G = \dot{\boldsymbol{F}}_G \boldsymbol{F}_G^{-1}. \tag{13}$$

The relative rate of change of the volume of the traction-free configuration of a differential volume element is

$$\mathrm{tr}(\boldsymbol{L}_G) = \frac{d\dot{v}_G}{dv_G} \tag{14}$$

with $\mathrm{tr}(\boldsymbol{L}_G)$ the trace of $\boldsymbol{L}_G$. As discussed above, we assume herein a constant spatial mass density ϱ in differential volume elements under any loading conditions and therefore also in their traction-free configuration. Therefore, the relative rate of change of the size of differential volume elements in the traction-free configuration must be equal to the relative rate of change of the mass in these volume elements, that is,

$$\frac{\dot{\varrho}_0}{\varrho_0} = \frac{d\dot{v}_G}{dv_G} = \mathrm{tr}(\boldsymbol{L}_G). \tag{15}$$

$\dot{\boldsymbol{F}}_G$ is associated with an elastic distension of the extant material while new material is squeezed in. To quantify it, we consider an infinitesimal change $d\boldsymbol{F}_G$ of the traction-free configuration that results from the deposition of an additional mass increment dm. The traction-free configuration of the material that has been in the differential volume element already before deposition of the mass increment dm does not change during the deposition process (recalling that herein we assume that growth and remodeling are separate processes, see also section 3). Let the elastic bulk stretch tensor of this material be $\boldsymbol{F}_E$. $\boldsymbol{F}_E$ maps between the traction-free configuration of the material existing before deposition of dm and its current traction-free configuration. By definition, before deposition of dm one has $\boldsymbol{F}_E = \boldsymbol{I}$. After

deposition of dm and the associated change of the traction-free configuration by $d\boldsymbol{F}_G$ one has $\boldsymbol{F}_E = \boldsymbol{I} + d\boldsymbol{F}_E$ with

$$(\boldsymbol{I} + d\boldsymbol{F}_E)\boldsymbol{F}_G = \boldsymbol{F}_G + d\boldsymbol{F}_G, \tag{16}$$

giving

$$d\boldsymbol{F}_E = d\boldsymbol{F}_G \boldsymbol{F}_G^{-1}. \tag{17}$$

Dividing (17) by the time increment dt over which the mass increment dm is deposited and using (13) yields

$$\dot{\boldsymbol{F}}_E = \boldsymbol{L}_G. \tag{18}$$

The rate of change of the elastic Cauchy-Green deformation tensor $\boldsymbol{C}_E = \boldsymbol{F}_E^T \boldsymbol{F}_E$ of the extant material during the growth process is thus (in a given traction-free configuration where the extant material exhibits a bulk elastic stretch tensor $\boldsymbol{F}_E = \boldsymbol{I}$)

$$\dot{\boldsymbol{C}}_E = \dot{\boldsymbol{F}}_E^T \boldsymbol{F}_E + \boldsymbol{F}_E^T \dot{\boldsymbol{F}}_E = \dot{\boldsymbol{F}}_E^T + \dot{\boldsymbol{F}}_E = 2\boldsymbol{D}_G \tag{19}$$

with

$$\boldsymbol{D}_G = \frac{1}{2}\left(\boldsymbol{L}_G + \boldsymbol{L}_G^T\right) \tag{20}$$

the symmetric part of the velocity gradient $\boldsymbol{L}_G$. Strain energy of the extant material in the neighborhood of a given traction-free configuration (in which we have $\boldsymbol{C}_E = \boldsymbol{I}$ for the extant material) can be expressed via a Taylor expansion as

$$\Psi(\boldsymbol{C}_E = \boldsymbol{I} + d\boldsymbol{C}_E) = \Psi(\boldsymbol{C}_E = \boldsymbol{I}) + \frac{\partial \Psi}{\partial \boldsymbol{C}_E} : d\boldsymbol{C}_E + \frac{1}{2}d\boldsymbol{C}_E : \frac{\partial^2 \Psi}{\partial \boldsymbol{C}_E^2} : d\boldsymbol{C}_E + o(d\boldsymbol{C}_E : d\boldsymbol{C}_E) \tag{21}$$

with the Lamdau symbol $o(.)$ and colons denoting double contraction products between tensors. By definition in the traction-free configuration $\partial \Psi / \partial \boldsymbol{C}_E = \boldsymbol{0}$. Then from (19) and (21) we conclude that the elastic energy of the material in a differential volume element changes during mass deposition over a time interval of length dt by the increment

$$d\Psi = \frac{1}{2}d\boldsymbol{C}_E : \frac{\partial^2 \Psi}{\partial \boldsymbol{C}_E^2} : d\boldsymbol{C}_E = 2dt^2 \boldsymbol{D}_G : \frac{\partial^2 \Psi}{\partial \boldsymbol{C}_E^2} : \boldsymbol{D}_G. \tag{22}$$

As can be seen from (15), the mass production rate per unit reference volume $\dot{\varrho}_0$ determines the rate of relative volumetric expansion of the traction-free configuration. But it does not enforce any specific shape of the traction-free configuration. As a consequence of the principle of minimum energy, the shape of the traction-free configuration will thus evolve such that $d\Psi$ is minimal. Let $d\Psi$ be minimal for $\boldsymbol{D}_G = \boldsymbol{D}_G^*$. Then

$$\boldsymbol{D}_G^* = \underset{\boldsymbol{D}_G}{\mathrm{argmin}}\left\{\boldsymbol{D}_G : \frac{\partial^2 \Psi}{\partial \boldsymbol{C}_E^2} : \boldsymbol{D}_G\right\}, \tag{23}$$

that is, $\boldsymbol{D}_G^*$ is the $\boldsymbol{D}_G$ which minimizes the term in the braces. Assuming a constant spatial mass density (as we do herein), using (15) and (20) in (23) leads to the constrained optimization problem

$$\boldsymbol{D}_G^* = \underset{\boldsymbol{D}_G \,:\, \mathrm{tr}(\boldsymbol{D}_G) = \dot{\varrho}_0/\varrho_0}{\mathrm{argmin}} \left\{ \boldsymbol{D}_G \; : \frac{\partial^2 \bar{\Psi}}{\partial \boldsymbol{C}_E^2} : \boldsymbol{D}_G \right\}. \tag{24}$$

where $\bar{\Psi} = \Psi - \Psi^*$ is the total strain energy minus the (isotropic) penalty energy Ψ^* modeling excluded volume interactions and ensuring constant spatial density. The fourth order stiffness tensor $\partial^2 \bar{\Psi}/\partial \boldsymbol{C}_E^2$ is symmetric and assumed here to be positive definite. Its inverse is the compliance tensor $\overline{\mathbb{S}}$. As shown in Appendix A, the unique solution to (24) is

$$\boldsymbol{D}_G^* = \frac{\dot{\varrho}_0}{\mathrm{tr}(\overline{\mathbb{S}} : \boldsymbol{I}) \, \varrho_0} \overline{\mathbb{S}} : \boldsymbol{I}. \tag{25}$$

The symmetric part $\boldsymbol{D}_G$ of the velocity gradient $\boldsymbol{L}_G$ indicates how fast the traction-free configuration of a differential volume element dilates in different directions, cf. also section 4.5.2 in (Gonzalez and Stuart 2008). For example, after a principal axis transformation the diagonal elements of $\boldsymbol{D}_G$ indicate the strain rate at which the traction-free configuration dilates along the principle axes. From (25) it is thus apparent that, as a rule of thumb, during volumetric growth differential volume elements will dilate elastically mainly in the direction(s) of maximal compliance, that is, of lowest stiffness. This can indeed be understood quite intuitively. The elastic dilatation associated directly with growth is a form of elastic swelling. The energetic cost for swelling, which implies a stretch of extant fibers, is obviously minimal in the direction(s) of lowest material stiffness of the extant material. This is also illustrated in Figure 3.

So far we have discussed in this section in a first step only the immediate elastic dilatation of differential volume elements associated with growth. In a second step, we now examine the remodeling that results from this perturbation of the elastic stress field. The elastic dilatation by growth increases the elastic stress in fibers by an amount that is directly proportional to the elastic stretch induced in fiber direction by $\boldsymbol{D}_G^*$. As the latter elastic fiber stretch is in softer directions higher than in stiffer directions of the material, also the difference of fiber stress from the homeostatic target value due to growth will be. The higher this difference, the faster inelastic remodeling according to (12). Therefore, growth will not only result in an immediate elastic dilatation of differential volume elements predominantly in the softest material direction(s) but also to a long-term inelastic remodeling predominantly in these direction(s).

Remark 6: note that the above derived natural anisotropy of volumetric growth and remodeling induced by the combination of anisotropic stiffness and tensional homeostasis can be captured only if the constant spatial mass density of the tissue is enforced by a penalty function such as $\Psi^\#$ in (7) rather than by a volumetric-deviatoric split of the deformation gradient as used in various previous articles about volumetric growth. The reason is that, when using a penalty function, dilatation of volume elements by deposition of mass automatically always affects the elastic stretch $\boldsymbol{F}_e^i$. Minimization of the associated strain energy ultimately yields (25) and thereby a growth anisotropy governed by the tissue stiffness. The situation is completely different when using a volumetric-deviatoric split of the deformation gradient in order to model a constant spatial density of the tissue in a way similar to standard models of material incompressibility during elastic deformation. In this case, growth will not result in any elastic energy as

long as it occurs isotropically and thus affects the volumetric part of the deformation gradient only (which does not appear in the strain energy function). Therefore, in this case the argument of minimal strain energy put forward above would not induce any kind of growth anisotropy dependent on the stiffness anisotropy but it would rather always lead to isotropic growth, which has indeed also been observed in computer simulations (Grytsan, Watton et al. 2015) but which is in contradiction to experimental observations in various tissues as discussed in more detail below.

Remark 7: above only the symmetric part $\boldsymbol{D}_G$ of the velocity gradient $\boldsymbol{L}_G$ is examined. A discussion of the anti-symmetric part, which describes the rotation of the traction-free configuration, is skipped since it is not essential for understanding the aspects of growth dynamics on which we decided to focus herein.

Remark 8: in the theory developed herein, the evolution of the traction-free configuration of differential volume elements is governed by a minimum energy principle as revealed by (23). This establishes some link between the ideas introduced herein and the work of (Gizzi, Cherubini et al. 2014, Pandolfi, Gizzi et al. 2016) where electro-mechanical coupling in soft biological tissues is modeled by an inelastic part of the deformation gradient, which is also determined via the minimization of a potential.

5 Examples

The discussion from section 4 can directly be applied to understand the experimentally observed volumetric growth and remodeling in a variety of different soft biological tissues in a very natural way as we will demonstrate in this section by several examples. The parameters used for the computational studies reported in the following subsections are all summarized in Appendix B.

5.1 Volumetric growth and remodeling in membrane-like tissues

In membrane-like tissues such as the bladder, the stomach, the small and large intestine or blood vessels the stiff, reinforcing collagen fibers are mainly oriented perpendicular to the wall-thickness direction (Schriefl, Zeindlinger et al. 2012). The wall-thickness direction is thus the by far most compliant direction. Our model thus predicts volumetric growth and remodeling mainly in wall-thickness direction in such tissues, which is indeed in good agreement with experimental observations as discussed in the following subsections.

5.1.1 Vascular growth and remodeling in hypertension

In blood vessels increased blood pressure is well-known to stimulate volumetric growth via deposition of additional collagen fibers. This growth mainly increases wall thickness rather than length or diameter of blood vessels (Berry and Greenwald 1976, Matsumoto and Hayashi 1994). So far to the authors' best knowledge no explanation has been proposed why this is the case, whereas the discussion in section 4 can explain this phenomenon in quite a natural way.

To underline the agreement between our theory and experiments, we present in this section the results of computer simulations based on our theory. Therein, the artery is modeled as a circular cylinder. Its wall is a constrained mixture of elastin, five collagen fiber families (circumferential, axial, diagonal, radial) and one circumferential smooth muscle fiber family. Geoemetry parameters, strain energy functions, and material parameters are taken from section 4.3 of (Braeu, Seitz et al. 2017) with just a few minor

14

modifications. All the details of the computational model are given in Appendix B.

Remodeling of collagen and smooth muscle is captured by the above equation (12), which is equivalent to equation (17) in (Braeu, Seitz et al. 2017). As in (Braeu, Seitz et al. 2017) we assume also herein no remodeling of elastin. In the mass production equation (11) we choose both for collagen and smooth muscle fiber families

$$\boldsymbol{k}_\sigma^i = k_\sigma^i \boldsymbol{A}^i \otimes \boldsymbol{A}^i. \tag{26}$$

with $\boldsymbol{A^i}$ the unit direction vector of the respective fiber families in reference configuration and

$$\Delta \boldsymbol{G}^i = \boldsymbol{R}^T \boldsymbol{\sigma}^i \boldsymbol{R} - \boldsymbol{\sigma}_h^i. \tag{27}$$

Here $\boldsymbol{\sigma}^i$ is the Cauchy stress of the i-th constituent, $\boldsymbol{\sigma}_h^i$ some constant homeostatic target stress, and $\boldsymbol{R}$ the rotational part of the deformation gradient $\boldsymbol{F}$. This choice of $\boldsymbol{k}_\sigma^i$ and $\Delta \boldsymbol{G}^i$ is equivalent to the one in (Braeu, Seitz et al. 2017).

In our simulations we mimic the experiment of (Berry and Greenwald 1976) where at some point in time $t = 0$ the artery is subjected to a sudden increase in blood pressure p from $100\ mmHg$ to $180\ mmHg$ and the subsequent growth and remodeling is observed over several weeks.

The results of our computer simulations are presented in In Figure 4 with $T^i = 7$ days in (12) and three different gain parameters $k_\sigma^i = 0.22/T^i$, $k_\sigma^i = 0.28/T^i$ and $k_\sigma^i = 0.34/T^i$ in (26). As expected from the discussion in section 4, the volumetric growth induced by hypertension mainly leads to a thickening of the arterial wall because the wall-thickness direction is by far the most compliant direction in the tissue. This is clearly visible by the relative change of the ratio between the mid-radius R_{mid}, the average between the inner and outer radius of the artery, and the wall thickness H over time, that is, by

$$\widehat{H}(t) = \frac{R_{mid}(t)/H(t) - R_{mid}(t = 0)/H(t = 0)}{R_{mid}(t = 0)/H(t = 0)} \ . \tag{28}$$

As apparent from Figure 4, for $k_\sigma^i = 0.28/T^i$ the ratio between wall thickening and radius dilation in the simulation at $t = 16$ weeks agrees well with the experimental observation reported by (Berry and Greenwald 1976). We thus note that the theory developed in this paper can – for an appropriate choice of parameters – excellently reproduce the kind of growth and remodeling observed in the vasculature without prescribing in any explicit way its specific anisotropy. In opposition to that, one can easily demonstrate that computational models where growth is prescribed to be an evolving isotropic inelastic deformation of differential volume elements, an approach that is frequently used in the literature, are in general unable to capture the growth and remodeling observed in arteries even qualitatively. The reason is that such models always produce a similar dilatation of the tissue in radial and circumferential direction, which is in clear contradiction to experimental observations.
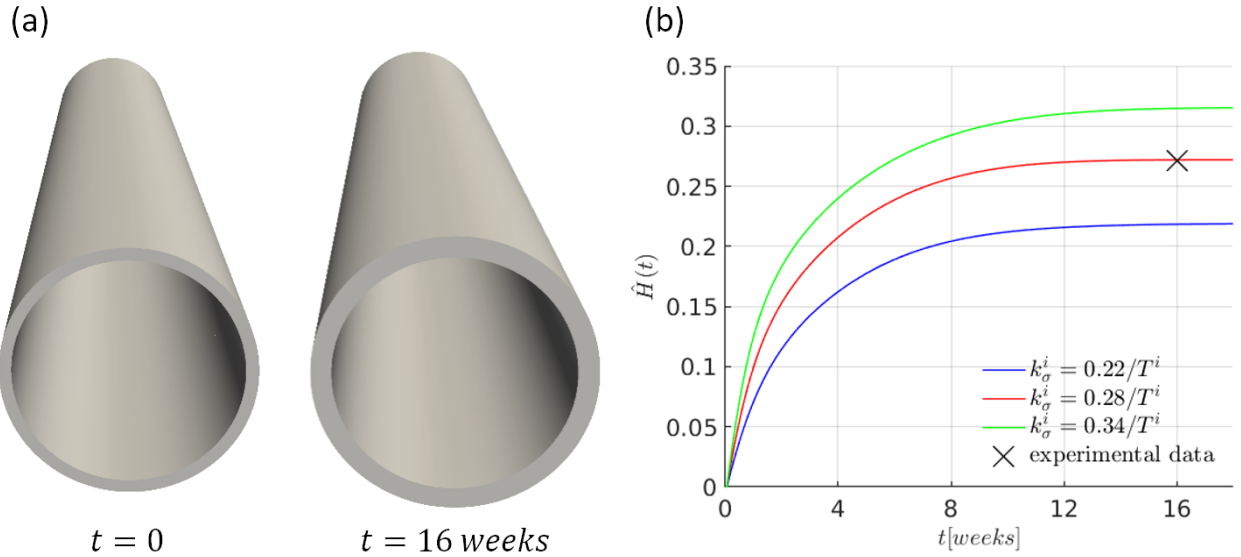
Figure 4: artery before (left) and after (right) increase of blood pressure from 100mmHg to 180mmHg subsequent to which both the diameter and the wall thickness increase by growth and remodeling. The relative change of the ratio $\hat{H}$ between wall thickness and vessel mid-radius over time is plotted for different simulated gain parameters and compared to experimental data from (Berry and Greenwald 1976)

5.1.2   Aneurysms

Aneurysms are local dilatations of the vascular wall. They typically enlarge over years and often finally rupture, which is one of the most common causes of death in industrialized countries. The initiation and enlargement of aneurysms remain poorly understood to date. Computer simulations are therefore increasingly used to study both. Here we present the simulation of an enlarging aneurysm (Figure 5) using the computational model described in section 5.1.1 but with $k_\sigma^i = 0.05/T^i$ and $T^i = 101$ days. Moreover, in the simulation, we keep the blood pressure at the initial value of 100mmHg and initiate the enlargement of the aneurysm by a damage to the elastin layer following equation (45) in Appendix B. This example demonstrates that our novel approach to volumetric growth and remodeling can capture volumetric growth and remodeling successfully not only in the mechanobiologically stable regime considered in section 5.1.1 but also in the mechanobiologically unstable regime governing the enlargement of aneurysms (Cyron and Humphrey 2014, Cyron, Wilson et al. 2014).
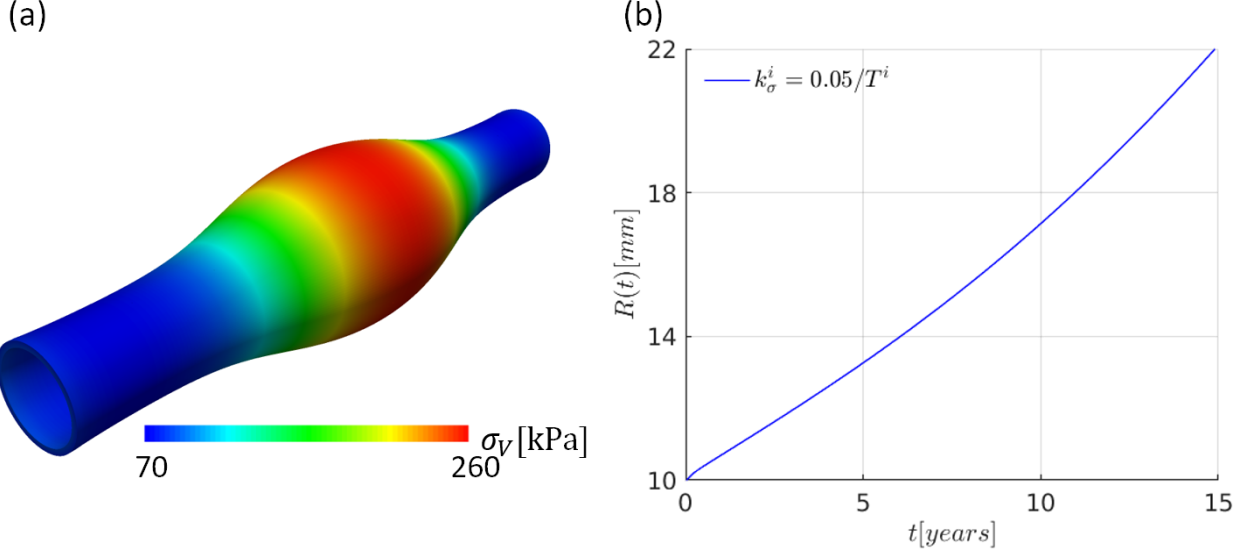
Figure 5: (a) von-Mises stress in an idealized fusiform abdominal aortic aneurysm 15 years after initiation. (b) Maximal inner radius of the aneurysm over time.

5.2 Volumetric growth in rope-like tissues

In rope-like tissues such as tendons or ligaments, volumetric growth by deposition of additional mass may occur, for example, due to inflammation, which induces deposition of ground matrix and swelling through attraction of water. This is well-known to result in thickening, that is, an increase in cross-section, rather than an increase in length or a substantial relaxation of axial tension (Bass 2012). Again, this phenomenon can be naturally explained from the discussion in section 4. The much higher stiffness in axial than transverse direction makes tendons and ligaments expand during volumetric growth mainly in transverse direction. To illustrate the ability of our theory to capture this phenomenon, we model the geometry of the tendon as a rectangular prism with three collagen fiber families aligned with its edges. Computer simulations are performed with a simple orthotropic material resembling the situation in tendons and ligaments at least qualitatively. In our computational model we used the strain energy

$$\Psi = \frac{\varrho_0^{gr}(t)}{\varrho_0^{gr}(t=0)} G[\mathrm{tr}(\overline{C}) - 3] + \frac{1}{2}\sum_i \frac{\varrho_0^i(t)}{\varrho_0^i(t=0)} \varphi^i E\big[\big(A_{gr}^i \otimes A_{gr}^i : C_e^i\big) - 1\big]^2 + \Psi^\#. \tag{29}$$

The isotropic Neo-Hookean energy which forms the first summand on the right-hand side of (29) represents the shear stiffness of the ground matrix (constituent superscript gr), which is assumed to be proportional to the tissue mass and be defined by the modulus $G = 13.85$ MPa taken from (Weiss, Maker et al. 1996). C is the Cauchy-Green deformation tensor and $\overline{C}$ its isochoric counterpart. The sum of quadratic functions which forms the second summand on the right-hand side represents three families of collagen fibers oriented in axial ($i = co(ax)$) and in the two transverse directions ($i = co(0°), co(90°)$). These are aligned with the unit direction vectors A_0^i in reference configuration and the unit direction vectors $A_{gr}^i = F_{gr}^i A_0^i / \|F_{gr}^i A_0^i\|$ in the inelastically deformed intermediate configuration. C_e^i is the elastic Cauchy-Green deformation tensor, $E = 125$ MPa the elastic modulus of the collagen fibers taken from

17

the one-dimensional model for ligaments proposed by (Yu, Walker et al. 2001), and φ^i the fraction of collagen fibers forming a specific fiber family. The penalty function $\Psi^{\#}$ from (10) is used with $\varepsilon = 300$ MPa. At time $t = 0$ the initial elastic stretch in fiber direction equals the respective homeostatic stretch which means that no mechano-regulated remodeling takes place at the start of the simulation. In general, remodeling in the ground matrix is assumed to be very slow, similar to the one of elastin in arteries, and thus neglected. By contrast, remodeling in the collagen fibers is much faster and therefore included in the simulation with a remodeling time constant $T^{co} = 24.5\ days$ in (12). We assume that at time $t = 0$ inflammatory processes start in the tissue, leading to deposition of additional mass, which is modeled herein as a special constituent of the constrained mixture with a referential mass density $\varrho_0^I(t)$ that increases from zero at time $t = 0$ to a value equal to the initial referential mass density of the healthy tissue at time $t = 6$ weeks. That is, within 6 weeks the total tissue mass is assumed to increase by a factor of two. Mass changes of the ground matrix and the collagen fibers happen on a very slow time scale compared to the mass changes due to inflammation and are therefore neglected in our simulation by choosing $\boldsymbol{k}_\sigma^i = \boldsymbol{0}$ for these constituents in (26). The additional mass deposited due to inflammation is assumed to be not load-bearing and does thus not appear in (29). To mimic the boundary conditions in vivo both ends of the idealized tendon are fixed in axial direction.

In Figure 6(a) we compare the initial geometry (opaque) with the geometry at time $t = 30$ weeks (transparent) when both mass deposition due to inflammation and the resulting remodeling of the collagen fibers are (largely) finished as apparent from Figure 6(b). Figure 6(b) shows the total collagen fiber stretch in axial and the two transverse directions compared to their inelastic counterparts $\lambda_{gr}^j = \sqrt{\boldsymbol{A}_0^j \otimes \boldsymbol{A}_0^j : \boldsymbol{C}_{gr}^j}$ with $\boldsymbol{C}_{gr}^j = \boldsymbol{F}_{gr}^{jT} \boldsymbol{F}_{gr}^j$.

Growth and remodeling illustrated in Figure 6 can be understood as follows. Due to the elastic deformation induced by volumetric growth over the first six weeks, collagen fiber stress increases. Following Eq. (12), the associated elastic fiber stretch is converted by remodeling into an inelastic stretch λ_{gr}^i. This inelastic fiber relaxation continues until the original homeostatic stress level in each collagen fiber family is restored. In Figure 6(b) we can see that this is for the transverse collagen fiber families by and large the case for $t \geq 20$ weeks. Altogether the deposition of additional mass due to inflammation leads for $t \geq 20$ weeks to a state where the cross section of the tendon has significantly grown. At the same time elastic stress in axial direction is on the same level as before. That is, the deposition of additional ground matrix has not induced a loss of axial tension in the tendon, which appears physiologically reasonable. We note that standard isotropic growth models are not able to reproduce this behavior. Rather in such models the growth of the tendon cross-section would necessarily be associated with considerable a loss of tension in axial direction for which, to the authors' best knowledge, so far no experimental evidence has been reported. While we have shown in this section that our growth model produces also for tendons results that appear physiologically reasonable, we also underline we have not been able to support our computational results by a quantitative comparison with experimental data due to a lack of such data in the literature. Performing such a quantitative comparison in collaboration with clinicians would be an important step to further evaluate the validity of the theory developed herein.
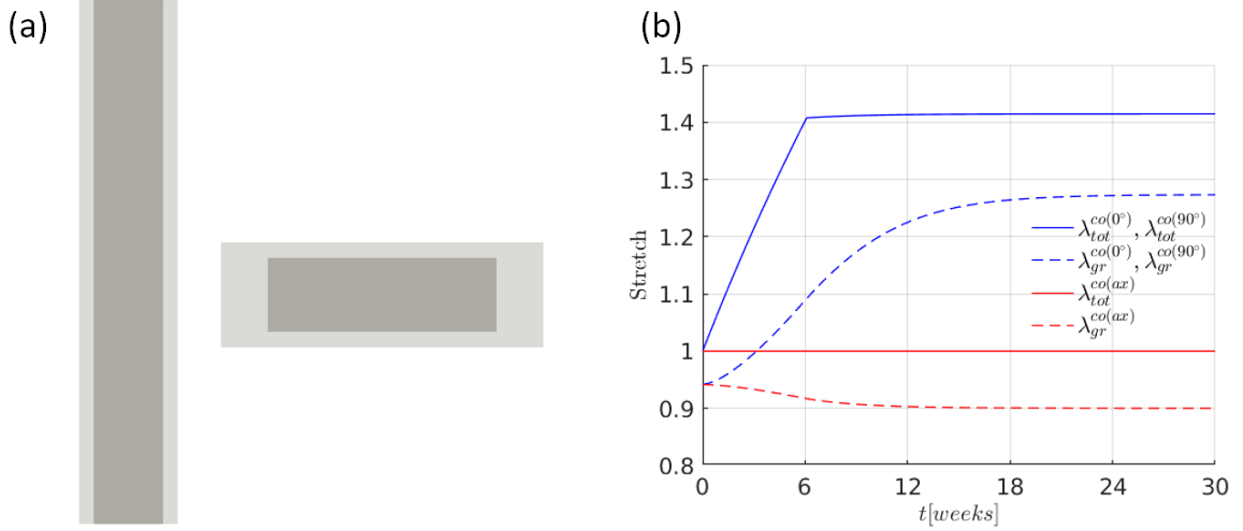
Figure 6: (a) axial section (left) and cross section (right) of initial geometry (opaque) vs. geometry at time $t = 30$ weeks after deposition of additional mass due to inflammation and remodeling of the collagen fibers (transparent).. Volumetric growth and remodeling gives rise to an equal dilatation of the volume in both directions perpendicular to the axis of the tendon. (b) Total ($\lambda_{tot}^{co(0°)}, \lambda_{tot}^{co(90°)}$) and inelastic collagen fiber stretch ($\lambda_{gr}^{co(0°)}, \lambda_{gr}^{co(90°)}$) in the two main transverse directions and total ($\lambda_{tot}^{co(ax)}$) and inelastic ($\lambda_{gr}^{co(ax)}$) collagen fiber stretch in axial direction over time.

5.3 Volumetric growth in (nearly) isotropic tissues

In rope-like tissues such as tendons and ligaments, stiffness in axial direction is around two orders of magnitude higher than in transverse direction (Yin and Elliott 2004). In membrane-like tissues such as blood vessels, stiffness in wall-thickness direction is around two orders of magnitude lower than in the other directions (Wilson, Baek et al. 2013). In addition to these two categories, there are also soft tissues, which exhibit a nearly isotropic stiffness. For example, the stiffness of liver lobules exhibits only a mild anisotropy with one direction by just around a factor of two stiffer than the other two directions (Chui, Kobayashi et al. 2007). In tissues with (nearly) isotropic stiffness we expect from the discussion in section 4 (nearly) isotropic volumetric growth and remodeling. To demonstrate this, we performed computer simulations of volumetric growth with the following isotropic strain energy function:

$$\Psi = \frac{\varrho_0^{gr}(t)}{\varrho_0^{gr}(t=0)} E^{gr} \left[\frac{1}{4(1+\nu^{gr})} \left(I_1 - 3 - 2\ln(|\boldsymbol{F}(t)|)\right) + \frac{\nu^{gr}}{2(1+\nu^{gr})(1-2\nu^{gr})} (|\boldsymbol{F}(t)| - 1)^2 \right]$$
$$+ \frac{1}{2} \frac{\varrho_0^{co}(t)}{\varrho_0^{co}(t=0)} E^{co} [(\boldsymbol{M}_{iso}^{co} : \boldsymbol{C}_e^{co}) - 1]^2 + \Psi^{\#}. \tag{30}$$

The first Neo-Hookean summand on the right hand side represents the ground matrix (constituent superscript gr) with the elastic modulus $E^{gr} = 1$ Pa and Poisson's ratio $\nu = 0.3$. The second quadratic summand on the right-hand side represents the collagen fibers (constitutent superscript co) with the elastic modulus $E^{co} = 10$ Pa and structural tensor $\boldsymbol{M}_{iso}^{co}$. By defining $\boldsymbol{M}_{iso}^{co}$ as a diagonal tensor with each term equal to $1/3$, the quadratic function in Eq. (30) represents an isotropic fiber distribution. Again the penalty function $\Psi^{\#}$ from (10) is used with a penalty parameter $\varepsilon = 1$ kPa.

In such a tissue, we model a growth process similar to the one studied in section 5.2. That is, we increase the total referential mass density $\varrho_0(t)$ by a factor of two over 10 weeks and assume that the newly

deposited mass is not load-bearing and does therefore not appear in the strain energy in Eq. (30). Additionally, we only consider remodeling of collagen fibers and neglect mass changes of the ground matrix and the collagen fibers, that is, $\boldsymbol{k}_\sigma^{gr} = \boldsymbol{k}_\sigma^{co} = \boldsymbol{0}$ in (11). We use a spheroidal initial geometry with radius R.

The result of the computer simulation of volumetric growth under these conditions is shown in Figure 7. As expected for a material with isotropic stiffness, the initially spheroidal body grows isotropically (see Figure 7(a)). Figure 7(b) shows that remodeling of the collagen fibers converts the elastic stretch induced by volumetric growth into an inelastic fiber stretch and after some time of adaptation. A new homeostatic state is reached in which the collagen fiber stress largely equals the homeostatic value again after around 30 weeks.

The computational example in this section was motivated by the problem of volumetric growth and remodeling in the liver or small tumors. Both kinds of tissue exhibit a nearly isotropic stiffness (Chui, Kobayashi et al. 2007, Jain, Martin et al. 2014) and in both volumetric growth is frequently observed. In the liver, this volumetric growth is associated with the pathology of hepatic steatosis, where fat accumulates in the liver cells. Clinically, one observes that both during tumor growth and in hepatic steatosis the tissue volume typically expands in all spatial directions approximately equally. Interestingly, this is exactly what one would expect from (23) and the discussion in section 4 for tissues with (nearly) isotropic stiffness. Saying this, we emphasize that we only point here at a surprising agreement between our theory and clinical observations in small tumors and the liver. We do, however, at this point not claim that the theory developed herein can fully explain volumetric growth and remodeling in small tumors or the liver. The reason for our caution is that the theory developed herein is crucially based on the assumption that microstructural reorganization (remodeling) is mainly governed by the principle of tensional homeostasis. While this idea is widely accepted for load-bearing soft tissues such as blood vessels, tendons or ligaments, it is so far unclear, to which extent (or whether at all) it is also applicable to tumor and liver tissue. At the same time, mass transport, the theory of porous media and some other more advanced aspects of modeling are neglected herein. These may, however, play important roles in the liver and tumors (Grillo, Federico et al. 2012, Mascheroni, Carfagna et al. 2018). Therefore, statements about the relation between the computational example in this section and growth and remodeling in the liver and small tumors should be made with great caution at this point. Hence, we limit our statement to simply pointing at the remarkable agreement between the results of our model and clinical observations made for liver or tumor growth.

(a)

(b)
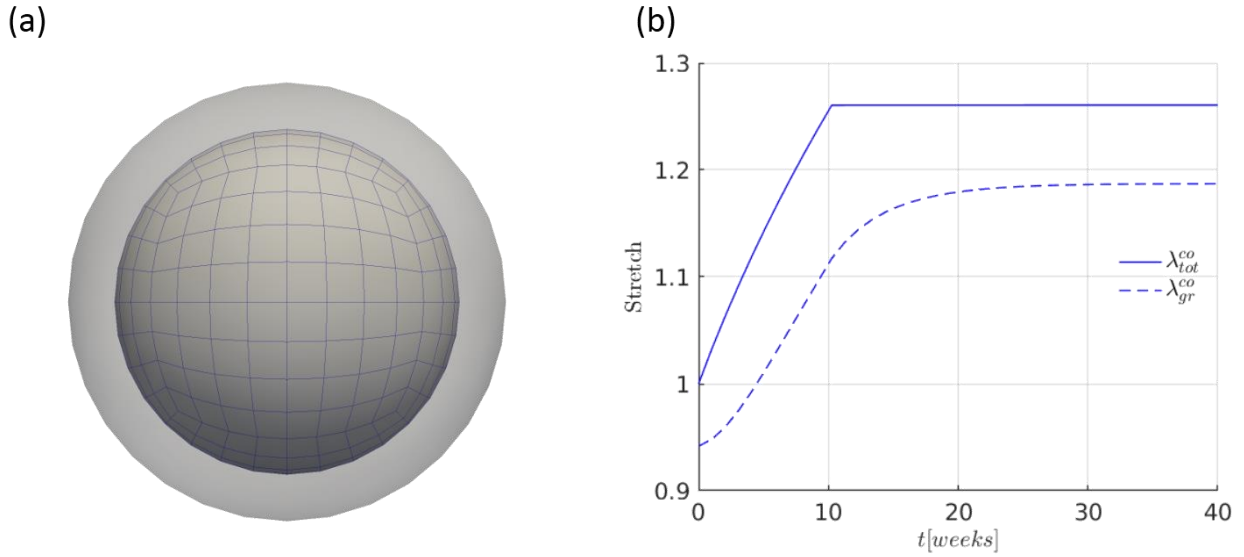
Figure 7: (a) volumetric growth in a spheroidal tissue with isotropic stiffness is isotropic, that is, it maps the initial geometry (opaque) on a dilated sphere (transparent). (b) Total stretch $\lambda_{tot}^{co} = R(t)/R(t=0)$ with radius R of the sphere and inelastic collagen fiber stretch λ_{gr}^{co} over time.

6 Discussion

Most previous work tries to capture volumetric growth in soft biological tissues by way of an inelastic part of the deformation gradient often referred to as growth tensor. This always leads to the important question how to define such a tensor, in particular its anisotropy. Unfortunately, there is so far no satisfactory answer to this question and thus most work relies on heuristic ad-hoc assumptions. To overcome this problem, we herein introduced a completely different approach. Our approach is based on two simple hypotheses. The first hypothesis is that during volumetric growth the total mass density of the tissue remains constant so that deposition of additional mass is automatically associated with an increase of tissue volume. The second hypothesis is that any reorganization of the elastic microstructure of the tissue, termed herein as remodeling, is governed by a single principle, the principle of tensional homeostasis. This principle has been identified over the last two decades by numerous studies as a key principle of soft tissue mechanobiology. It is therefore general rather than specific for a particular kind of soft tissue. In section 4 we demonstrated that the above two simple hypotheses directly give rise to what one may consider a natural anisotropy of volumetric growth and remodeling. That is, in the absence of any additional confounding factors volumetric growth and remodeling will, as a rule of thumb, result in an expansion of differential tissue volume elements mainly in the direction(s) of lowest stiffness. In section 5 we demonstrated that this natural anisotropy of volumetric growth and remodeling agrees very well with the anisotropy observed experimentally in a variety of different soft tissues ranging from blood vessels over tendons to tissues with a rather isotropic stiffness.

This means that the new approach introduced herein can explain the anisotropy of volumetric growth and remodeling observed experimentally in a host of different tissues from just two simple and general hypotheses, which are both supported by experimental observations and which are applicable to a large range of load-bearing collagenous soft biological tissues. In opposition to that, previous models of growth

21

and remodeling based on the concept of an inelastic growth tensor had to come up for each specific kind of tissue with a tissue-specific definition of this growth tensor which was usually of a rather heuristic kind and not based on general or fundamental principles.

The growth theory developed herein has an interesting consequence regarding adaptation of living tissues to external loading. It is well-known that fibers in living tissues have a natural tendency to rotate into the direction of mechanical loading. This naturally increases stiffness in loading direction. The theory developed herein then predicts that deposition of additional mass will automatically happen mainly in compliant tissue direction(s), that is, mainly perpendicular to the loading direction(s), which automatically increases the load-bearing cross section and thereby the strength of the tissue in the most efficient way. The natural relation between stiffness and growth, which is the main result of this article, may help to understand better not only growth and remodeling during mechano-adaptation of adult tissues but also during morphogenesis. Especially during morphogenesis it remains hard to measure and also hard to model the complex and often anisotropic changes of the tissue geometry. The theory developed herein may offer a simple way to understand and predict these changes from stiffness, which is a quantity that can be measured and modeled often quite accurately. This means that further attempts to model the stiffness of biological tissues more accurately, following for example (Gasser, Ogden et al. 2006, Vasta, Gizzi et al. 2014, Gizzi, Pandolfi et al. 2016, Niestrawska, Viertler et al. 2016, Gizzi, Pandolfi et al. 2017, Holzapfel and Ogden 2017), might in the future also be very helpful to understand better complex patterns of volumetric growth.

While the results shown in the examples section of this paper are promising, further studies are definitely required in order to decide to which extent the theory developed in this paper can capture the physiology of volumetric growth in different soft tissues realistically. Moreover, it might be an interesting avenue of future research to extend the theory developed herein such that it includes also the biochemical processes and transport processes that drive volumetric growth in biological tissues, for example along the lines of (Grillo, Federico et al. 2012, Marino, Pontrelli et al. 2017, Mascheroni, Carfagna et al. 2018).

Acknowledgments

Compliance with ethical standards

Conflict of interest: the authors declare that they have no conflict of interest.

Appendix A

In this appendix we demonstrate how to solve the constrained minimization problem (24) analytically. To this end, we introduce a Lagrangian multiplier λ so that the constrained minimization problem can be reduced to an unconstrained minimization of the Lagrange functional

$$\mathcal{L}(\boldsymbol{D}_G^*, \lambda^*) = \boldsymbol{D}_G : \frac{\partial^2 \overline{\Psi}}{\partial \boldsymbol{C}_E^2} : \boldsymbol{D}_G + \lambda \left[tr(\boldsymbol{D}_G) - \frac{\dot{\varrho}_0}{\varrho_0} \right] \tag{31}$$

Finding a minimum (or maximum) of (31) is equivalent to finding a stationary point of the Lagrange functional $\mathcal{L}$. Let at this stationary point $\boldsymbol{D}_G$ and λ take on the values $\boldsymbol{D}_G^*$ and λ^*, respectively. Then

$$\frac{\partial \mathcal{L}}{\partial \boldsymbol{D}_G}(\boldsymbol{D}_G^*, \lambda^*) = 2 \frac{\partial^2 \overline{\Psi}}{\partial \boldsymbol{C}_E^2} : \boldsymbol{D}_G^* + \lambda^* \boldsymbol{I} = \boldsymbol{0}, \tag{32}$$

$$\frac{\partial \mathcal{L}}{\partial \lambda}(\boldsymbol{D}_G^*, \lambda^*) = tr(\boldsymbol{D}_G^*) - \frac{\dot{\varrho}_0}{\varrho_0} = 0. \tag{33}$$

(32) yields

$$\boldsymbol{D}_G^* = -\frac{1}{2} \lambda^* \overline{\mathbb{S}} : \boldsymbol{I}. \tag{34}$$

with the fourth-order compliance tensor

$$\overline{\mathbb{S}} = \left[\frac{\partial^2 \overline{\Psi}}{\partial \boldsymbol{C}_E^2} \right]^{-1}. \tag{35}$$

Using (34) in (33) gives

$$\lambda^* = -\frac{2\dot{\varrho}_0}{tr(\overline{\mathbb{S}} : \boldsymbol{I}) \varrho_0}, \tag{36}$$

and using (36) in (34)

$$\boldsymbol{D}_G^* = \frac{\dot{\varrho}_0}{tr(\overline{\mathbb{S}} : \boldsymbol{I}) \varrho_0} \overline{\mathbb{S}} : \boldsymbol{I} \tag{37}$$

Note that $\boldsymbol{D}_G^*$ marks a minimum rather than a maximum of $\mathcal{L}$ and thereby of the elastic energy cost by volumetric growth due to the positive definiteness of the stiffness $\partial^2 \overline{\Psi}/\partial \boldsymbol{C}_E^2$ assumed herein.

Appendix B

In this appendix we summarize all relevant parameters and equations required to reproduce the simulations shown in the examples section 5. In section 5.1.1 and section 5.1.2 we model the arterial wall as a constrained mixture of elastin, circumferential smooth muscle and, unlike to (Braeu, Seitz et al. 2017), five collagen fiber families. (Schriefl, Zeindlinger et al. 2012) showed that the orientation of collagen fibers is in general not perfectly aligned with the tangential plane of the aortic wall but rather may exhibit also a small radial component. To account for this phenomenon, we included in the constitutive model of the wall an additional collagen fiber family in wall thickness direction with a small reference mass density. In the following, the superscripts el, co, and sm are used for quantities referring to elastin, collagen, and smooth muscle, respectively. The total strain energy of elastin per unit mass is assumed to be given by the sum

$$W^{el} = W_{2D}^{el} + W_{3D}^{el} \tag{38}$$

with the isotropic two-dimensional Neo-Hookean strain energy function

$$W_{2D}^{el} = \frac{\mu_{2D}^{el}}{2}\left[\boldsymbol{C}_e^{el}:\boldsymbol{A}_{gr}^{\parallel} + \frac{1}{\left|\boldsymbol{A}_{gr}^{\parallel}\boldsymbol{C}_e^{el}\boldsymbol{A}_{gr}^{\parallel} + \boldsymbol{A}_{gr}^{\perp}\right|} - 3\right].$$

(39)

Here μ_{2D}^{el} is a stiffness parameter, $\boldsymbol{A}_{gr}^{rad} = \boldsymbol{a}_{gr}^{rad}\otimes\boldsymbol{a}_{gr}^{rad}$ the structural tensor in wall thickness direction with $\boldsymbol{a}_{gr}^{rad}$ the unit vector in wall thickness direction in the intermediate configuration of elastin, $\boldsymbol{A}_{gr}^{\parallel} = \boldsymbol{I} - \boldsymbol{a}_{gr}^{rad}\otimes\boldsymbol{a}_{gr}^{rad}$ is the structural tensor for the axial-circumferential plane in the vessel wall. The second strain energy contribution of elastin is the compressible isotropic three-dimensional Neo-Hookean strain energy

$$W_{3D}^{el} = \frac{E^{el}}{4(1 + \nu^{el})}\left(\text{tr}\left(\boldsymbol{C}_e^{el}\right) - 3 - 2\ln\left(\left|\boldsymbol{F}_e^{el}(t)\right|\right)\right) + \frac{E^{el}\nu^{el}}{2(1 + \nu^{el})(1 - 2\nu^{el})}\left(\left|\boldsymbol{F}_e^{el}(t)\right| - 1\right)^2$$

(40)

with the specific elastic modulus E^{el} and Poisson's ratio ν^{el}. The strain energy per unit mass of each collagen fiber family is modeled with a Fung-type exponential function

$$W^{co} = \frac{k_1^{co}}{2k_2^{co}}\left(e^{k_2^{co}(I_a^{co}-1)^2} - 1\right)$$

(41)

with material parameters k_1^{co} and k_2^{co}, and I_a^{co} the square of the elastic stretch of the respective collagen fiber family. The strain energy of smooth muscle per unit mass is the sum

$$W^{sm} = W_{pas}^{sm} + W_{act}^{sm}$$

(42)

of a passive Fung-type part

$$W_{pas}^{sm} = \frac{k_1^{sm}}{2k_2^{sm}}\left(e^{k_2^{sm}(I_a^{sm}-1)^2} - 1\right)$$

(43)

with material parameters k_1^{sm} and k_2^{sm}, and I_a^{sm} the square of the elastic stretch of the smooth muscle fiber family, and an active part

$$W_{act}^{sm} = \frac{\sigma_{actm}^{sm}}{\varrho_0(t=0)}\left(\lambda_{act}^{sm} + \frac{1}{3}\frac{(\lambda_m^{sm} - \lambda_{act}^{sm})^3}{(\lambda_m^{sm} - \lambda_0^{sm})^2}\right)$$

(44)

with λ_{act}^{sm} the active stretch in fiber direction, σ_{actm}^{sm} the maximal active Cauchy stress, and λ_m^{sm} and λ_0^{sm} the active stretches at maximum and zero active stress. Herein, we assume that $\partial\lambda_{act}^{sm}/\partial\lambda^{sm} = 1/\lambda^{sm}$ with λ^{sm} the total stretch of the smooth muscle fibers compared to the reference configuration, which is important to calculate the stress resulting from (44). Additionally, we add a penalty-type strain energy as given in Eq. (10) with the penalty parameter given in Table 1. In section 5.1.2 the vessel is initially in equilibrium and all fibers are in a homeostatic state. At time $t = 0$ this homeostatic state is perturbed by spatially distributed damage to the elastin layer that progresses over time with the damage rate

$$\dot{D}^{el}(\boldsymbol{X},t) = -\frac{1}{T^{el}}\varrho_0^{el}(\boldsymbol{X},t) - \left[\frac{D_{max}}{t_{dam}}\exp\left[-0.5\left(\frac{X_3}{L_{dam}}\right)^2\right]\exp\left[-\frac{t}{t_{dam}}\right]\right]\varrho_0^{el}(\boldsymbol{X},0)$$

(45)

where a coordinate system is used with the origin in the center of the cylinder and the X_3-axis aligned with the symmetry axis of the cylinder. Table 1 summarizes the simulation parameters used both in

section 5.1.1 and section 5.1.2. The parameters that differ between section 5.1.1 and section 5.1.2 are presented separately in Table 2 and Table 3.

Mesh		
Element type		8-noded hexahedral linear finite elements
Element technology		F-bar method to avoid locking (de Souza Neto, Perić et al. 1996)
Number of elements		165,888
Geometry / Load		
Inner radius of cylinder	R	10 mm
Wall thickness of cylinder	H	1.41 mm
Length of cylinder	L	180mm
Blood pressure on inner wall of cylinder	p	100 mmHg
Material parameters		
Elastin: 2D Neo-Hookean parameter	μ_{2D}^{el}	∈[71 ; 104] J/kg
Elastin: 3D Neo-Hookean elastic modulus	E^{el}	72 J/kg
Elastin: 3D Neo-Hookean Poisson's ratio	ν^{el}	0.3
Collagen: Fung exponential parameters	k_1^{co}	568 J/kg
	k_2^{co}	11.2
Smooth muscle: passive contribution	k_1^{sm}	7.6 J/kg
	k_2^{sm}	11.4
Smooth muscle: active contribution	σ_{actm}^{sm}	54 kPa
	λ_0^{sm}	0.8
	λ_m^{sm}	1.4
	λ_{act}^{sm}	1
Penalty parameter	ε	150 kPa
Initial reference mass densities		
Elastin	$\varrho_0^{el}(t=0)$	241.5 kg/m^3
Collagen: circumferential	$\varrho_0^{co(cir)}(t=0)$	61.845 kg/m^3
Collagen: axial	$\varrho_0^{co(ax)}(t=0)$	61.845 kg/m^3
Collagen: diagonal	$\varrho_0^{co(diag)}(t=0)$, $\varrho_0^{co(-diag)}(t=0)$	247.38 kg/m^3
Collagen: radial	$\varrho_0^{co(rad)}(t=0)$	32.55 kg/m^3
Smooth muscle	$\varrho_0^{sm}(t=0)$	157.5 kg/m^3
Total initial reference mass density	$\varrho_0(t=0)$	1050 kg/m^3
Growth and remodeling parameters		
Elastin: mean life time	T^{el}	101 years
Elastin: gain parameter	k_σ^{el}	0
Initial elastic stretch (equal to homeostatic stretch / deposition stretch for collagen and smooth muscle)		
Elastin: axial direction	$\lambda_e^{el(ax)}(t=0)$	1.25
Elastin: circumferential direction	$\lambda_e^{el(cir)}(t=0)$	1.34
Elastin: radial direction	$\lambda_e^{el(rad)}(t=0)$	∈[0.29 ; 0.51]
Collagen (in fiber direction)	$\lambda_e^{co}(t=0)$	1.062
Smooth muscle (in fiber direction)	$\lambda_e^{sm}(t=0)$	1.10

Table 1: Shared simulation parameters of the idealized cylindrical blood vessel studied in section 5.1.1 and 5.1.2. To distinguish between the different collagen fiber families we use, when appropriate, superscripts *co(ax)*, *co(cir)*, *co(diag)*, *co(-diag)*, and *co(rad)* for circumferential, axial, diagonal, and radial collagen fibers. The homeostatic stretch in fiber direction of collagen and smooth muscle equals the elastic stretch in the initial configuration. To ensure mechanical and mechanobiological equilibrium in the initial configuration the parameters $\boldsymbol{\mu}_{2D}^{el}$ and $\boldsymbol{\lambda}_e^{el(rad)}(\boldsymbol{t=0})$ are varied in the initial configuration in wall thickness direction according to the procedure described in Appendix A of (Braeu, Seitz et al. 2017).

Simulation		
Time step size	Δt	0.34 days
Load		
Mean blood pressure jump	Δp	80 mmHg
Growth and remodeling parameters		
Collagen/ Smooth muscle: turnover time	$T^{co} = T^{sm}$	7 days
Collagen/ Smooth muscle: gain parameter	$k_\sigma^{co} = k_\sigma^{sm}$	[0.22, 0.28, 0.34]/T^{co}

Table 2: Additional simulation parameters for the idealized cylindrical blood vessel studied in section 5.1.1.

Simulation		
Time step size	Δt	5 days
Growth and remodeling parameters		
Collagen/ Smooth muscle: turnover time	$T^{co} = T^{sm}$	101 days
Collagen/ Smooth muscle: gain parameter	$k_\sigma^{co} = k_\sigma^{sm}$	0.05/T^{co}
Damage parameters in model aneurysm		
Damage spread in space	L_{dam}	10 mm
Damage spread in time	t_{dam}	40 days
Maximal damage	D_{max}	0.5

Table 3: Additional simulation parameters for the idealized cylindrical blood vessel studied in section 5.1.2.

In section 5.2, we studied the growth of an idealized tendon due to inflammation. The size of the geometry was motivated by values reported in the literature for Achilles tendons. To model the elastic behavior of tendons at least qualitatively we used the strain energy function from (30) and the simulation parameters summarized in Table 4.

Simulation		
Time step size	Δt	3 days
Mesh		
Element type		8-noded hexahedral finite elements
Element technology		F-bar method to avoid locking (de Souza Neto, Perić et al. 1996)
Number of elements		384
Geometry		
Width	B	13.3 mm (Mello, Marchiori et al. 2006)
Thickness	H	4.3 mm (Aydın, Filippucci et al. 2014)
Length	L	100 mm
Reference mass densities		
Healthy tissue	$\varrho_0^H(t) = const$	1050 kg/m^3
Mass produced due to inflammation	$\varrho_0^I(t > 6\ weeks) = const$	1050 kg/m^3
Material parameters		
Ground matrix: Neo-Hookean shear parameter	G	13.85 MPa (Weiss, Maker et al. 1996)
Collagen: mass fraction in axial direction	$\varphi^{co(ax)}$	90 %
Collagen: mass fraction in transverse directions	$\varphi^{co(0°)}, \varphi^{co(90°)}$	5 %
Collagen: stiffness parameter	E	125 MPa
Penalty parameter	ε	300 MPa
Remodeling parameters		
Ground matrix: mean life time	T^m	101 years

Collagen: turnover time	T^{co}	24.5 days
Initial elastic stretch (equal to homeostatic stretch / deposition stretch)		
Collagen (in fiber direction)	$\lambda_e^{co}(t=0)$	1.062

Table 4: Simulation parameters of the simplified tendon model studied in section 5.2.

In section 5.3 we studied growth of a spheroidal tissue with the simulation parameters from Table 5.

Simulation		
Time step size	Δt	7 days
Mesh		
Element type		8-noded hexahedral finite elements
Element technology		F-bar method to avoid locking (de Souza Neto, Perić et al. 1996)
Number of elements		2048
Geometry		
Initial radius	R	10 mm
Reference mass densities		
Healthy tissue	$\varrho_0^H(t) = const$	1050 kg/m^3
Newly deposited mass	$\varrho_0^D(t > 10\ weeks) = const$	1050 kg/m^3
Material parameters		
Ground matrix: elastic modulus	E	1 Pa
Ground matrix: Poisson's ratio	ν^{gr}	0.3
Collagen: stiffness parameter	E^{co}	10 Pa
Penalty-type function	ε	1 kPa
Remodeling parameters		
Ground matrix: mean life time	T^m	101 years
Collagen: turnover time	T^{co}	1 year (Decaris, Emson et al. 2015)
Initial elastic stretch (equal to homeostatic stretch / deposition stretch)		
Collagen (in fiber direction)	$\lambda_e^{co}(t=0)$	1.062

Table 5: Simulation parameters of the spheroidal tissue studied in section 5.3.

References

Ambrosi, D., G. A. Ateshian, E. M. Arruda, S. C. Cowin, J. Dumais, A. Goriely, G. A. Holzapfel, J. D. Humphrey, R. Kemkemer, E. Kuhl, J. E. Olberding, L. A. Taber and K. Garikipati (2011). "Perspectives on biological growth and remodeling." J Mech Phys Solids **59**(4): 863-883.

Ambrosi, D. and F. Guana (2007). "Stress-modulated growth." Mathematics and mechanics of solids **12**(3): 319-342.

Aydın, S. Z., E. Filippucci, P. Atagündüz, Ş. Yavuz, W. Grassi and H. Direskeneli (2014). "Sonographic measurement of Achilles tendon thickness in seronegative spondyloarthropathies." European Journal of Rheumatology **1**(1): 7-10.

Bass, E. (2012). "Tendinopathy: why the difference between tendinitis and tendinosis matters." International journal of therapeutic massage & bodywork **5**(1): 14.

Berry, C. L. and S. E. Greenwald (1976). "Effects of hypertension on the static mechanical properties and chemical composition of the rat aorta1." Cardiovascular Research **10**(4): 437-451.

Braeu, F. A., A. Seitz, R. C. Aydin and C. J. Cyron (2017). "Homogenized constrained mixture models for anisotropic volumetric growth and remodeling." Biomechanics and Modeling in Mechanobiology **16**(3): 889-906.

Braeu, F. A., A. Seitz, R. C. Aydin and C. J. Cyron (2017). "Homogenized constrained mixture models for anisotropic volumetric growth and remodeling." Biomech Model Mechanobiol.

Brown, R. A., R. Prajapati, D. A. McGrouther, I. V. Yannas and M. Eastwood (1998). "Tensional homeostasis in dermal fibroblasts: mechanical responses to mechanical loading in three-dimensional substrates." J Cell Physiol **175**(3): 323-332.

Chui, C., E. Kobayashi, X. Chen, T. Hisada and I. Sakuma (2007). "Transversely isotropic properties of porcine liver tissue: experiments and constitutive modelling." Medical & Biological Engineering & Computing **45**(1): 99-106.

Cyron, C. and R. Aydin (2017). "Mechanobiological free energy: a variational approach to tensional homeostasis in tissue equivalents." ZAMM-Journal of Applied Mathematics and Mechanics/Zeitschrift für Angewandte Mathematik und Mechanik **97**(9): 1011-1019.

Cyron, C. J., R. C. Aydin and J. D. Humphrey (2016). "A homogenized constrained mixture (and mechanical analog) model for growth and remodeling of soft tissue." Biomechanics and Modeling in Mechanobiology **15**(6): 1389-1403.

Cyron, C. J. and J. D. Humphrey (2014). "Vascular homeostasis and the concept of mechanobiological stability." International Journal of Engineering Science **85**(0): 203-223.

Cyron, C. J. and J. D. Humphrey (2017). "Growth and remodeling of load-bearing biological soft tissues." Meccanica **52**(3): 645-664.

Cyron, C. J., J. S. Wilson and J. D. Humphrey (2014). "Mechanobiological stability: a new paradigm to understand the enlargement of aneurysms?" Journal of The Royal Society Interface **11**(100): 20140680.

de Souza Neto, E. A., D. Perić, M. Dutko and D. R. J. Owen (1996). "Design of simple low order finite elements for large strain analysis of nearly incompressible solids." International Journal of Solids and Structures **33**(20): 3277-3296.

Decaris, M. L., C. L. Emson, K. Li, M. Gatmaitan, F. Luo, J. Cattin, C. Nakamura, W. E. Holmes, T. E. Angel, M. G. Peters, S. M. Turner and M. K. Hellerstein (2015). "Turnover Rates of Hepatic Collagen and Circulating Collagen-Associated Proteins in Humans with Chronic Liver Disease." PLoS ONE **10**(4): e0123311.

DiCarlo, A., S. Naili and S. Quiligotti (2006). "Sur le remodelage des tissus osseux anisotropes." Comptes Rendus Mécanique **334**(11): 651-661.

DiCarlo, A. and S. Quiligotti (2002). "Growth and balance." Mechanics Research Communications **29**(6): 449-456.

Eriksson, T. S. E., P. N. Watton, X. Y. Luo and Y. Ventikos (2014). "Modelling volumetric growth in a thick walled fibre reinforced artery." Journal of the Mechanics and Physics of Solids **73**: 134-150.

Ezra, D. G., J. S. Ellis, M. Beaconsfield, R. Collin and M. Bailly (2010). "Changes in fibroblast mechanostat set point and mechanosensitivity: an adaptive response to mechanical stress in floppy eyelid syndrome." Invest Ophthalmol Vis Sci **51**(8): 3853-3863.

Flynn, B. P., A. P. Bhole, N. Saeidi, M. Liles, C. A. DiMarzio and J. W. Ruberti (2010). "Mechanical strain stabilizes reconstituted collagen fibrils against enzymatic degradation by mammalian collagenase matrix metalloproteinase 8 (MMP-8)." PLoS One **5**(8): e12337.

Gasser, T. C., R. W. Ogden and G. A. Holzapfel (2006). "Hyperelastic modelling of arterial layers with distributed collagen fibre orientations." Journal of The Royal Society Interface **3**(6): 15-35.

Gizzi, A., C. Cherubini, S. Filippi and A. Pandolfi (2014). "Theoretical and Numerical Modeling of Nonlinear Electromechanics with applications to Biological Active Media." Communications in Computational Physics **17**(1): 93-126.

Gizzi, A., A. Pandolfi and M. Vasta (2016). "Statistical characterization of the anisotropic strain energy in soft materials with distributed fibers." Mechanics of Materials **92**(Supplement C): 119-138.

Gizzi, A., A. Pandolfi and M. Vasta (2017). "A generalized statistical approach for modeling fiber-reinforced materials." Journal of Engineering Mathematics.

Gonzalez, O. and A. M. Stuart (2008). A First Course in Continuum Mechanics. Cambridge, Cambridge University Press.

Goriely, A. and R. Vandiver (2010). "On the mechanical stability of growing arteries." IMA journal of applied mathematics **75**: 549-570.

Grillo, A., S. Federico and G. Wittum (2012). "Growth, mass transfer, and remodeling in fiber-reinforced, multi-constituent materials." International Journal of Non-Linear Mechanics **47**(2): 388-401.

Grytsan, A., T. Eriksson, P. Watton and T. Gasser (2017). "Growth Description for Vessel Wall Adaptation: A Thick-Walled Mixture Model of Abdominal Aortic Aneurysm Evolution." Materials **10**(9): 994.

Grytsan, A., T. S. E. Eriksson, P. N. Watton and T. C. Gasser (2017). "Growth Description for Vessel Wall Adaptation: A Thick-Walled Mixture Model of Abdominal Aortic Aneurysm Evolution." Materials (Basel) **10**(9).

Grytsan, A., P. N. Watton and G. A. Holzapfel (2015). "A Thick-Walled Fluid–Solid-Growth Model of Abdominal Aortic Aneurysm Evolution: Application to a Patient-Specific Geometry." Journal of biomechanical engineering **137**(3): 031008.

Grytsan, A., P. N. Watton and G. A. Holzapfel (2015). "A Thick-Walled Fluid–Solid-Growth Model of Abdominal Aortic Aneurysm Evolution: Application to a Patient-Specific Geometry." Journal of Biomechanical Engineering **137**(3): 031008-031008.

Grytz, R., G. Meschke and J. B. Jonas (2011). "The collagen fibril architecture in the lamina cribrosa and peripapillary sclera predicted by a computational remodeling approach." Biomech Model Mechanobiol **10**(3): 371-382.

Grytz, R., I. A. Sigal, J. W. Ruberti, G. Meschke and J. C. Downs (2012). "Lamina Cribrosa Thickening in Early Glaucoma Predicted by a Microstructure Motivated Growth and Remodeling Approach." Mech Mater **44**: 99-109.

Holzapfel, G. (2000). Nonlinear Solid Mechanics: A Continuum Approach for Engineering, John Wiley & Sons Ltd.

Holzapfel, G. A. and R. W. Ogden (2017). "Comparison of two model frameworks for fiber dispersion in the elasticity of soft biological tissues." European Journal of Mechanics - A/Solids **66**(Supplement C): 193-200.

Humphrey, J. D., E. R. Dufresne and M. A. Schwartz (2014). "Mechanotransduction and extracellular matrix homeostasis." Nat Rev Mol Cell Biol **15**(12): 802-812.

Humphrey, J. D. and K. R. Rajagopal (2002). "A constrained mixture model for growth and remodeling of soft tissues." Mathematical Models and Methods in Applied Sciences **12**(03): 407-430.

Jain, R. K., J. D. Martin and T. Stylianopoulos (2014). "The role of mechanical forces in tumor growth and therapy." Annual review of biomedical engineering **16**: 321-346.

Karšaj, I., J. Sorić and J. D. Humphrey (2010). "A 3-D framework for arterial growth and remodeling in response to altered hemodynamics." Int J Eng Sci **48**(11): 1357-1372.

Kehl, S. and M. W. Gee (2017). "Calibration of parameters for cardiovascular models with application to arterial growth." International Journal for Numerical Methods in Biomedical Engineering **33**(5): e2822-n/a.

Lin, W. J., M. D. Iafrati, R. A. Peattie and L. Dorfmann (2017). "Growth and remodeling with application to abdominal aortic aneurysms." Journal of Engineering Mathematics.

Lindquist Liljeqvist, M., R. Hultgren, T. C. Gasser and J. Roy (2016). "Volume growth of abdominal aortic aneurysms correlates with baseline volume and increasing finite element analysis-derived rupture risk." J Vasc Surg **63**(6): 1434-1442.e1433.

Marino, M., G. Pontrelli, G. Vairo and P. Wriggers (2017). "A chemo-mechano-biological formulation for the effects of biochemical alterations on arterial mechanics: the role of molecular transport and multiscale tissue remodelling." Journal of The Royal Society Interface **14**(136).

Mascheroni, P., M. Carfagna, A. Grillo, D. Boso and B. Schrefler (2018). "An avascular tumor growth model based on porous media mechanics and evolving natural states." Mathematics and Mechanics of Solids **23**(4): 686-712.

Matsumoto, T. and K. Hayashi (1994). "Mechanical and dimensional adaptation of rat aorta to hypertension." J Biomech Eng **116**(3): 278-283.

Matsumoto, T. and K. Hayashi (1996). Response of arterial wall to hypertension and residual stress. Biomechanics. K. Hayashi, A. Kamiya and K. Ono, Springer**:** 93 - 119.

Mello, R. A. F. d., E. Marchiori, A. A. S. M. D. d. Santos and G. Torres Neto (2006). "Avaliação morfométrica do tendão de Aquiles por ultra-sonografia." Radiologia Brasileira **39**: 161-165.

Menzel, A. and E. Kuhl (2012). "Frontiers in growth and remodeling." Mechanics Research Communications **42**(0): 1-14.

Niestrawska, J. A., C. Viertler, P. Regitnig, T. U. Cohnert, G. Sommer and G. A. Holzapfel (2016). "Microstructure and mechanics of healthy and aneurysmatic abdominal aortas: experimental analysis and modelling." Journal of The Royal Society Interface **13**(124).

Pandolfi, A., A. Gizzi and M. Vasta (2016). "Coupled electro-mechanical models of fiber-distributed active tissues." Journal of biomechanics **49**(12): 2436-2444.

Rodriguez, E. K., A. Hoger and A. D. McCulloch (1994). "Stress-dependent finite growth in soft elastic tissues." J Biomech **27**(4): 455-467.

Sáez, P., E. Peña, M. A. Martínez and E. Kuhl (2014). "Computational modeling of hypertensive growth in the human carotid artery." Computational mechanics **53**(6): 1183-1196.

Schriefl, A. J., G. Zeindlinger, D. M. Pierce, P. Regitnig and G. A. Holzapfel (2012). "Determination of the layer-specific distributed collagen fibre orientations in human thoracic and abdominal aortas and common iliac arteries." J R Soc Interface **9**(71): 1275-1286.

Schriefl, A. J., G. Zeindlinger, D. M. Pierce, P. Regitnig and G. A. Holzapfel (2012). "Determination of the layer-specific distributed collagen fibre orientations in human thoracic and abdominal aortas and common iliac arteries." Journal of The Royal Society Interface **9**(71): 1275-1286.

Skalak, R., D. A. Farrow and A. Hoger (1997). "Kinematics of surface growth." Journal of Mathematical Biology **35**(8): 869-907.

Soleimani, M., P. Wriggers, H. Rath and M. Stiesch (2016). "Numerical simulation and experimental validation of biofilm in a multi-physics framework using an SPH based method." Computational Mechanics **58**(4): 619-633.

Truster, T. J. and A. Masud (2017). "A unified mixture formulation for density and volumetric growth of multi-constituent solids in tissue engineering." Computer Methods in Applied Mechanics and Engineering **314**: 222-268.

Tsamis, A., A. Cheng, T. C. Nguyen, F. Langer, D. C. Miller and E. Kuhl (2012). "Kinematics of cardiac growth: in vivo characterization of growth tensors and strains." J Mech Behav Biomed Mater **8**: 165-177.

Valentín, A., J. Humphrey and G. A. Holzapfel (2013). "A finite element-based constrained mixture implementation for arterial growth, remodeling, and adaptation: Theory and numerical verification." International journal for numerical methods in biomedical engineering **29**(8): 822-849.

Vasta, M., A. Gizzi and A. Pandolfi (2014). "On three- and two-dimensional fiber distributed models of biological tissues." Probabilistic Engineering Mechanics **37**(Supplement C): 170-179.

Virag, L., J. S. Wilson, J. D. Humphrey and I. Karsaj (2017). "Potential biomechanical roles of risk factors in the evolution of thrombus-laden abdominal aortic aneurysms." Int J Numer Method Biomed Eng **33**(12).

Watton, P., N. Hill and M. Heil (2004). "A mathematical model for the growth of the abdominal aortic aneurysm." Biomechanics and modeling in mechanobiology **3**(2): 98-113.

Weiss, J. A., B. N. Maker and S. Govindjee (1996). "Finite element implementation of incompressible, transversely isotropic hyperelasticity." Computer Methods in Applied Mechanics and Engineering **135**(1): 107-128.

Wilson, J. S., S. Baek and J. D. Humphrey (2012). "Importance of initial aortic properties on the evolving regional anisotropy, stiffness and wall thickness of human abdominal aortic aneurysms." J R Soc Interface **9**(74): 2047-2058.

Wilson, J. S., S. Baek and J. D. Humphrey (2013). "Parametric study of effects of collagen turnover on the natural history of abdominal aortic aneurysms." Proc. R. Soc. A **469**(2150): 20120556.

Wolinsky, H. and S. Glagov (1967). "A lamellar unit of aortic medial structure and function in mammals." Circ Res **20**(1): 99-111.

Yin, L. and D. M. Elliott (2004). "A biphasic and transversely isotropic mechanical model for tendon: application to mouse tail fascicles in uniaxial tension." J Biomech **37**(6): 907-916.

Yu, C.-H., P. S. Walker and M. E. Dewar (2001). "The effect of design variables of condylar total knees on the joint forces in step climbing based on a computer model." Journal of Biomechanics **34**(8): 1011-1021.

Zöllner, A. M., O. J. Abilez, M. Böl and E. Kuhl (2012). "Stretching skeletal muscle: chronic musde lengthening through sarcomerogenesis." PLoS One **7**(10): e45661.